International Journal of Innovative Computing, Information and Control
Volume **8**, Number **3(B)**, March **2012**

ICIC International ©2012 ISSN 1349-4198
pp. 2375–2388

LONG BASELINE GNSS RELATIVE POSITIONING WITH ESTIMATING IONOSPHERIC AND TROPOSPHERIC DELAYS AND THEIR GRADIENTS

Yukihiro Kubo, Hisaya Tanaka, Masaharu Ohashi and Sueo Sugimoto

Department of Electrical and Electronic Engineering
Ritsumeikan University
1-1-1, Noji-Higashi, Kusatsu City, Shiga 525-8577, Japan
ykubo@se.ritsumei.ac.jp

Received March 2011; revised July 2011

Abstract. *In the long baseline GPS (Global Positioning System)/GNSS (Global Navigation Satellite System) relative positioning the ionospheric and tropospheric delays are dominant factors for the positioning accuracy. In this paper, we present Real Time Kinematic (RTK) relative positioning algorithms for long baselines with simultaneously estimating ionospheric and tropospheric delays and their gradients. Also some dynamical models [1-3] of the rover station are reviewed for applying Kalman filters, and we show the experimental results of relative positioning for various baselines (short, medium, long) by using the Gps Earth Observation NETwork (GEONET) data provided by Geospatial Information Authority (GSI) of Japan.*
Keywords: GNSS regression models, Ionospheric delay, VTEC, GEONET, Orthogonal polynomials

1. **Introduction.** The GNSS relative positioning is one of the positioning methods which can provide most precise relative position between a receiver at a known point (reference station) and a receiver at a unknown point (rover station). In general relative positioning method, the unknown position is estimated by using so-called double differences of pseudorange and carrier phase measurements obtained by the receivers [4, 5].

Generally, the dominant error sources of the estimated unknown position are the ionospheric and tropospheric delays of waves from satellites. However, if the distance between the receivers is not so long (generally less than 20 [km]), they can be canceled out by applying the double differencing technique because the propagation paths of the waves can be assumed to be almost the same, so that the ionospheric and tropospheric delays also can be assumed to be almost the same.

On the other hand, the double differencing technique is no longer effective for the medium and long baselines (more than 20 [km]) positioning due to large differences of the ionospheric and the tropospheric delays between the reference and rover GNSS receiver stations. For long baseline positioning, it is extremely important to obtain accurate information of the ionospheric and tropospheric delays in order to achieve rapid and accurate positioning results. Therefore, in this paper we propose the long baseline relative positioning algorithms with simultaneously estimating the ionospheric and tropospheric delays and their gradients at the reference and rover stations as the state variables in the Kalman filter.

In our previous research [6, 7], for the tropospheric delays, we have applied the formula which expresses the total tropospheric delay as the sum of the zenith hydrostatic and wet delays multiplied by mapping functions. Then we assume that the zenith hydrostatic

delay is given by the Saastamoinen model where the zenith wet delay is treated as an unknown parameter and it is estimated simultaneously in the position calculations. As an extension of our previous research, in this paper, we focus on the horizontal deformation of the tropospheric delays in the lower atmosphere by using the inhomogeneous mapping function, which models the effects of water vapor horizontal deformation as the gradient of the first order plane [8]. It seems to be effective for the mitigation of the horizontal component of the tropospheric delays. Therefore, the improvement of the horizontal positioning accuracy is expected by considering the horizontal deformation.

For the ionospheric delays, there exist several methods for mitigating their effects. The Klobuchar model [9] represents the zenith ionospheric delay as a constant value at night-time and a half-cosine function in day-time with a maximum at 2PM local time. However, the Klobuchar model can mitigate only approximately 50% rms errors of the ionospheric delays. As another method, the IGS (International GNSS Service) has been providing the total electron content (TEC) of ionosphere on a global scale. The IGS products known as GIM (Global Ionospheric Model) can provide better results than the Klobuchar model using the same GPS dataset and ephemeris [10].

On the other hand, the method to estimate the ionospheric effect within the positioning model has also been investigated [6, 7]. Therefore, we also estimate the ionospheric effects by using the same way as tropospheric delay. Mapping functions are used to map the zenith ionospheric delay to slant delays. And the ionospheric delays for all satellites are modeled by using the zenith delays and mapping functions at the reference and rover stations.

Furthermore, horizontal gradients in the east and north directions are modeled by using inhomogeneous mapping function. Then the ionospheric delays and ionospheric horizontal gradients are estimated by the Kalman filter. For applying the Kalman filter, state models for the zenith ionospheric delay and horizontal gradients are needed. Therefore, in this paper, both of the zenith ionospheric delay and horizontal gradients are assumed as a Brownian motion process (Wiener process) or a first order Markov process.

The proposed long baseline relative positioning algorithms with estimating ionospheric and tropospheric delays and their gradients provide highly rapid and accurate positioning. The experimental results under various circumstances such as static, kinematic environments and several lengths of baselines are shown in this paper.

2. **Mathematical Models.** We use the following mathematical models of the integrated pseudorange and carrier phase measurements for satellite p and the moving receiver u, namely, for static and kinematic positioning. When two receivers k and u obtain the pseudorange and carrier phase measurements from two satellites p and q, the double differenced pseudoranges $\rho^{pq}_{CA,ku}$ and $\rho^{pq}_{PY,ku}$ based on C/A and P(Y) codes and double differenced carrier phases $\varphi^{pq}_{L1,ku}$ and $\varphi^{pq}_{L2,ku}$ based on the $L1$ and $L2$ frequency carrier phases are given as follows [4, 5, 11]:

$$\rho^{pq}_{CA,ku}(t) = r^{pq}_{ku}(t) + \delta I^{pq}_{ku}(t) + \delta T^{pq}_{ku}(t) + e^{pq}_{CA,ku}(t), \tag{1}$$

$$\rho^{pq}_{PY,ku}(t) = r^{pq}_{ku}(t) + \frac{f_1^2}{f_2^2}\delta I^{pq}_{ku}(t) + \delta T^{pq}_{ku}(t) + e^{pq}_{PY,ku}(t), \tag{2}$$

$$\Phi^{pq}_{L1,ku}(t) = r^{pq}_{ku}(t) - \delta I^{pq}_{ku}(t) + \delta T^{pq}_{ku}(t) + \lambda_1 N^{pq}_{L1,ku} + \lambda_1 \varepsilon^{pq}_{L1,ku}(t), \tag{3}$$

$$\Phi^{pq}_{L2,ku}(t) = r^{pq}_{ku}(t) - \frac{f_1^2}{f_2^2}\delta I^{pq}_{ku}(t) + \delta T^{pq}_{ku}(t) + \lambda_2 N^{pq}_{L2,ku} + \lambda_2 \varepsilon^{pq}_{L2,ku}(t), \tag{4}$$

where

$$\delta I^{pq}_{ku} \equiv (\delta I^{p}_{k} - \delta I^{p}_{u}) - (\delta I^{q}_{k} - \delta I^{q}_{u}), \tag{5}$$

$$\delta T_{ku}^{pq} \equiv (\delta T_k^p - \delta T_u^p) - (\delta T_k^q - \delta T_u^q), \tag{6}$$
$$N_{L1,ku}^{pq} \equiv (N_{L1,k}^p - N_{L1,u}^p) - (N_{L1,k}^q - N_{L1,u}^q), \tag{7}$$
$$N_{L2,ku}^{pq} \equiv (N_{L2,k}^p - N_{L2,u}^p) - (N_{L2,k}^q - N_{L2,u}^q), \tag{8}$$
$$e_{CA,ku}^{pq} \equiv (e_{CA,k}^p - e_{CA,u}^p) - (e_{CA,k}^q - e_{CA,u}^q), \tag{9}$$
$$e_{PY,ku}^{pq} \equiv (e_{PY,k}^p - e_{PY,u}^p) - (e_{PY,k}^q - e_{PY,u}^q), \tag{10}$$
$$\varepsilon_{L1,ku}^{pq} \equiv \lambda_1 \Big[(\varepsilon_{L_1,k}^p - \varepsilon_{L_1,u}^p) - (\varepsilon_{L_1,k}^q - \varepsilon_{L_1,u}^q) \Big], \tag{11}$$
$$\varepsilon_{L2,ku}^{pq} \equiv \lambda_2 \Big[(\varepsilon_{L_2,k}^p - \varepsilon_{L_2,u}^p) - (\varepsilon_{L_2,k}^q - \varepsilon_{L_2,u}^q) \Big], \tag{12}$$

where t is the signal reception time, f_1, and f_2 are $L1$ and $L2$ carrier frequencies, (namely 1575.42 and 1227.60 [MHz] respectively). δI_{ku}^{pq} and δT_{ku}^{pq} are double differenced ionospheric and tropospheric propagation delays respectively. $\varepsilon_{L1,ku}^{pq}$, $\varepsilon_{L2,ku}^{pq}$, $\varepsilon_{CA,ku}^{pq}$ and $\varepsilon_{PY,ku}^{pq}$ denote the observation noises. Also $N_{L1,u}^p$ and $N_{L2,u}^p$ are the integer ambiguities, which are unknown integer numbers associated with the ambiguity of $L1$ and $L2$ carrier cycles at the initial time. λ_1 and λ_2 denote the wave lengths of the $L1$ and $L2$ carrier waves. $r_u^p(t)$ denotes the distance between the satellite p at the time $t - \tau_u^p$ and the receiver u at the time t; where τ_u^p denotes the traveling time of the carrier wave from the satellite p to the receiver u, namely,

$$\begin{aligned} r_{ku}^{pq} &\equiv (r_k^p - r_u^p) - (r_k^q - r_u^q), \\ &= \sqrt{(x_k - x^p)^2 + (y_k - y^p)^2 + (z_k - z^p)^2} \\ &\quad - \sqrt{(x_u - x^p)^2 + (y_u - y^p)^2 + (z_u - z^p)^2} \\ &\quad - \sqrt{(x_k - x^q)^2 + (y_k - y^q)^2 + (z_k - z^q)^2} \\ &\quad + \sqrt{(x_u - x^q)^2 + (y_u - y^q)^2 + (z_u - z^q)^2}. \end{aligned} \tag{13}$$

Thus, the 1st order Taylor series approximation of Equation (13) around the estimated value $u^p = \hat{u}^p$ is given by:

$$\begin{aligned} r_{ku}^{pq} &\approx r_{k\hat{u}^{(j)}}^{pq} + \left[\frac{\partial r_{ku}^{pq}}{\partial u} \right]_{u=\hat{u}^{(j)}}^{\mathrm{T}} \left(u - \hat{u}^{(j)} \right) \\ &= r_{k\hat{u}^{(j)}}^{pq} + g_{k\hat{u}^{(j)}}^{pq} \left(u - \hat{u}^{(j)} \right). \end{aligned} \tag{14}$$

At the short baseline occasion, the magnitude of the ionospheric and tropospheric delays included in the measurements can be assumed to be almost identical in the reference and the rover stations. Namely, we can assume

$$\delta I_{ku}^{pq} \approx 0, \quad \delta T_{ku}^{pq} \approx 0. \tag{15}$$

Therefore, Equations (1)-(4) can be approximated as follows;

$$\rho_{CA,ku}^{pq}(t) \approx r_{ku}^{pq}(t) + e_{CA,ku}^{pq}(t), \tag{16}$$
$$\rho_{PY,ku}^{pq}(t) \approx r_{ku}^{pq}(t) + e_{PY,ku}^{pq}(t), \tag{17}$$
$$\Phi_{L1,ku}^{pq}(t) \approx r_{ku}^{pq}(t) + \lambda_1 N_{L1,ku}^{pq} + \lambda_1 \varepsilon_{L1,ku}^{pq}(t), \tag{18}$$
$$\Phi_{L2,ku}^{pq}(t) \approx r_{ku}^{pq}(t) + \lambda_2 N_{L2,ku}^{pq} + \lambda_2 \varepsilon_{L2,ku}^{pq}(t). \tag{19}$$

However, at the medium or long baseline occasion, we can not assume the relations in Equation (15). There is a problem that the positioning accuracy is degraded if the ionospheric and the tropospheric delays in the double difference measurements are not properly removed.

Therefore, by using Equations (1)-(4), we propose the long baseline relative positioning algorithms with estimating simultaneously ionospheric delays at the reference and rover stations as the state variables and by utilizing parametric models for tropospheric delays.

3. Tropospheric Delay Models.

3.1. **Hydrostatic delays and wet delays.** The tropospheric delay can be considerable for satellites at low elevations. Unlike the ionosphere, the troposphere is not a dispersive medium and it causes the same delay for different frequencies. The tropospheric delay is normally represented as comprising a wet delay and a hydrostatic delay. The wet delay is difficult to model because of local variations in the water-vapor content of the troposphere and accounts for approximately 10% of the tropospheric delay. The hydrostatic delay is relatively well modeled and accounts for approximately 90% of the tropospheric delay [6].

The tropospheric zenith total delay (ZTD) $\delta T_{z,u}$ can be expressed as the sum of the zenith hydrostatic delay (ZHD) $\delta T_{zh,u}$ and zenith wet delay (ZWD) $\delta T_{zw,u}$ as follows (see Figure 1) [4, 12]:

$$\delta T_{z,u} = \delta T_{zh,u} + \delta T_{zw,u}. \tag{20}$$

Then, the slant total delay can be expressed using mapping functions, as follows:

$$\delta T_u^p = M_{h,u}^p \delta T_{zh,u} + M_{w,u}^p \delta T_{zw,u}, \tag{21}$$

$$M_{h,u}^p = \frac{1}{\sin(E_u^p) + \frac{0.00143}{\tan(E_u^p)+0.0445}}, \tag{22}$$

$$M_{w,u}^p = \frac{1}{\sin(E_u^p) + \frac{0.00035}{\tan(E_u^p)+0.017}}, \tag{23}$$

where $M_{h,u}^p$ and $M_{w,u}^p$ are the mapping functions for the hydrostatic and wet components, respectively. E_u^p is the elevation angle of the pth satellite.

Then, the zenith hydrostatic delay is given by the Saastamoinen model [4, 13]:

$$\delta T_{zh,u} = 0.002277(1 + 0.0026\cos 2\phi_u + 0.00028h_u)P_0, \tag{24}$$

where ϕ_u and h_u [km] denote the latitude and altitude, respectively, of the position of the receiver, and P_0 [mbar] denotes the atmospheric pressure. The zenith total delay is also treated as an unknown parameter.

3.2. **Tropospheric gradients.** When the low elevation data are applied, the variation of the horizontal tropospheric delay increases as it can not be neglected for precise positioning. Furthermore it may cause relatively large errors in the positioning results. In this paper, therefore, the horizontal deformation of the tropospheric delay is applied in the estimation of the tropospheric delays. Then, by using mapping functions which is modelled as tropospheric gradients, we estimate tropospheric gradients and correct them.

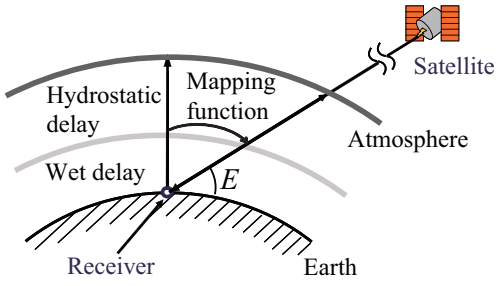

FIGURE 1. Mapping function for troposephere

The delay in the GPS signal due to the tropospheric gradient can be modelled as,

$$\delta T_G(E_u^p, A_u^p) = \delta T_{ns} M_{Ta}(E_u^p) \cos A_u^p + \delta T_{ew} M_{Ta}(E_u^p) \sin A_u^p, \tag{25}$$

where

$$M_{Ta}(E_u^p) = \frac{1}{\sin E_u^p \tan E_u^p + 0.0032}, \tag{26}$$

where δT_{ns}, and δT_{ew} are the gradients of north-south and east-west directions, A_u^p is an azimuth, and $M_{Ta}(E_u^p)\cos A_u^p$, $M_{Ta}(E_u^p)\sin A_u^p$ are the inhomogeneous mapping functions [7].

In this paper, therefore, the slant total tropospheric delay between the satellite p and receiver u, δT_u^p, in Equation (21) is replaced by the sum of the slant hydrostatic, wet delays and the gradients as follows:

$$\delta T_u^p = M_{h,u}^p \delta T_{zh,u} + M_{w,u}^p \delta T_{zw,u} + \delta T_{ns} M_{Ta}(E_u^p) \cos A_u^p + \delta T_{ew} M_{Ta}(E_u^p) \sin A_u^p, \tag{27}$$

where

$$M_h \equiv \begin{bmatrix} M_h^1 \\ M_h^2 \\ \vdots \\ M_h^{n_s} \end{bmatrix}, \quad M_w \equiv \begin{bmatrix} M_w^1 \\ M_w^2 \\ \vdots \\ M_w^{n_s} \end{bmatrix}. \tag{28}$$

Therefore, the double difference of tropospheric delay can be expressed as follows:

$$\begin{aligned}
\delta T_{ku}^{pq} &\equiv (\delta T_k^p - \delta T_u^p) - (\delta T_k^q - \delta T_u^q) \\
&= (M_{h,k}^{pq} \delta T_{zh,k} - M_{h,u}^{pq} \delta T_{zh,u}) - (M_{w,k}^{pq} \delta T_{zh,k} - M_{w,u}^{pq} \delta T_{zh,u}) \\
&\quad + (M_{w,k}^{pq} \delta T_{z,k} - M_{w,u}^{pq} \delta T_{z,u}) + (M_{T_{ns},k}^{p} \delta T_{ns,k}^{p} + M_{T_{ew},k}^{p} \delta T_{ew,k}^{p}) \\
&\quad - (M_{T_{ns},u}^{p} \delta T_{ns,u}^{p} - M_{T_{ew},u}^{p} \delta T_{ew,u}^{p}) - (M_{T_{ns},k}^{q} \delta T_{ns,k}^{q} - M_{T_{ew},k}^{q} \delta T_{ew,k}^{q}) \\
&\quad - (M_{T_{ns},u}^{q} \delta T_{ns,u}^{q} - M_{T_{ew},u}^{q} \delta T_{ew,u}^{q}) \\
&= (M_{h,k}^{pq} \delta T_{zh,k} - M_{h,u}^{pq} \delta T_{zh,u}) - (M_{w,k}^{pq} \delta T_{zh,k} - M_{w,u}^{pq} \delta T_{zh,u}) \\
&\quad + (M_{w,k}^{pq} \delta T_{z,k} - M_{w,u}^{pq} \delta T_{z,u}) + (M_{T_{ns},k}^{pq} \delta T_{ns,k} - M_{T_{ew},u}^{pq} \delta T_{ns,u}) \\
&\quad + (M_{T_{ew},k}^{pq} \delta T_{ew,k} - M_{T_{ew},u}^{pq} \delta T_{ew,u}),
\end{aligned} \tag{29}$$

where

$$M_{T_{ns},*} \equiv \begin{bmatrix} M_{az}^1 \cos A_*^1 \\ M_{az}^2 \cos A_*^2 \\ \vdots \\ M_{az}^{n_s} \cos A_*^{n_s} \end{bmatrix}, \quad M_{T_{ew},*} \equiv \begin{bmatrix} M_{az}^1 \sin A_*^1 \\ M_{az}^2 \sin A_*^2 \\ \vdots \\ M_{az}^{n_s} \sin A_*^{n_s} \end{bmatrix}. \tag{30}$$

4. **Ionospheric Delay Models.** The ionosphere is one of the biggest error sources in GPS positioning. Although dual frequency users can resolve this problem by using an ionosphere-free combination, ionospheric models for single-frequency users have not been well developed yet as described in Section 1. Therefore, in this research, by using inhomogeneous mapping function, we estimate ionospheric delays and correct them.

4.1. **Ionospheric delays.** The slant ionospheric delay $\delta I_u^p(E_u^p)$ can be expressed by using the zenith ionospheric delay (ZID) δI_z and mapping function $M_{I,u}(E_u^p)$ as follows:

$$\delta I_u^p = M_{I,u}(E_u^p) \delta I_{z,u}, \tag{31}$$

where

$$M_{I,u}(E_u^p) = \frac{1}{\sqrt{1 - \left(\frac{R_E}{R_E+H}\cos E_u^p\right)^2}}, \tag{32}$$

Here, the single-layer model shown in Figure 2 is applied. R_E ($\approx 6,371$ [km]) indicates the mean earth radius, and H is the height of the single layer.

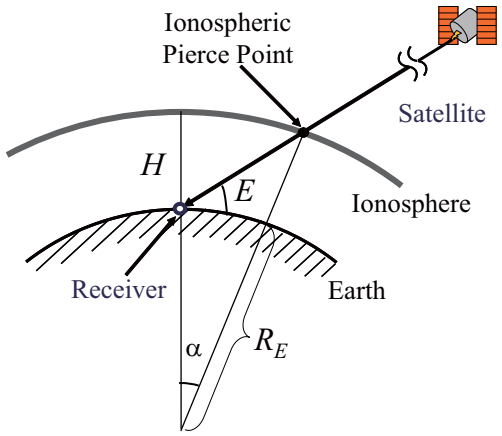

FIGURE 2. Single-layer model for ionosphere

4.2. **Ionospheric gradients.** In the previous section, for the modelling of the tropospheric delays, their gradients are considered to make them more accurate. The idea of gradients can be also applied to the modelling of the ionospheric delays. The delay due to the ionospheric gradient can be modeled by [14]

$$\delta I_{G,u}(E_u^p, A_u^p) = \delta I_{ns,u} M_{I,u}(E_u^p)\cot E_u^p \cos A_u^p + \delta I_{ew,u} M_{I,u}(E_u^p)\cot E_u^p \sin A_u^p, \tag{33}$$

where $I_{ns,u}$ and $I_{ew,u}$ are the horizontal gradients in the north and east directions, and $M_{I,u}(E_u^p)\cot E_u^p \cos A_u^p$ and $M_{I,u}(E_u^p)\cot E_u^p \sin A_u^p$ are the inhomogeneous mapping function.

In this paper, therefore, the slant ionospheric delay between the satellite p and receiver u, δI_u^p in Equation (31) is replaced by

$$\delta I_u^p = M_{I,u}(E_u^p)\delta I_{z,u} + \delta I_{G,u}^p(E_u^p, A_u^p). \tag{34}$$

For the estimation of the ionospheric delays, in this paper, zenith delay of the single differences of ionosphere between two receiver stations and their gradients are treated as unknown parameters. The ionospheric total delay can be expressed as follows:

$$\begin{aligned}
\delta I_{ku}^{pq} &\equiv (\delta I_k^p - \delta I_u^p) - (\delta I_k^q - \delta I_u^q) \\
&= \{(M_{I,k}^p \delta I_{z,k}^p + \delta I_{G,k}^p) - (M_{I,u}^p \delta I_{z,u}^p + \delta I_{G,u}^p)\} - \{(M_{I,k}^q \delta I_{z,k}^q + \delta I_{G,k}^q) \\
&\quad - (M_{I,u}^q \delta I_{z,u}^q + \delta I_{G,u}^q)\} \\
&= (M_{I,k}^p \delta I_{z,k}^p + M_{F_{ns},k}^p \delta I_{ns,k}^p + M_{F_{ew},k}^p \delta I_{ew,k}^p) - (M_{I,u}^p \delta I_{z,u}^p + M_{F_{ns},u}^p \delta I_{ns,u}^p \\
&\quad + M_{F_{ew},u}^p \delta I_{ew,u}^p) - (M_{I,k}^q \delta I_{z,k}^q + M_{F_{ns},k}^q \delta I_{ns,k}^q + M_{F_{ew},k}^q \delta I_{ew,k}^q) \\
&\quad + (M_{I,u}^q \delta I_{z,u}^q + M_{F_{ns},u}^q \delta I_{ns,u}^q + M_{F_{ew},u}^q \delta I_{ew,u}^q) \\
&\approx M_{I,k}^p \delta I_{z,ku}^p - M_{I,k}^q \delta I_{z,ku}^q + M_{F_{ns},k}^{pq} \delta I_{ns,k} + M_{F_{ew},k}^{pq} \delta I_{ew,k} \\
&\quad - M_{F_{ns},u}^{pq} \delta I_{ns,u} - M_{F_{ew},u}^{pq} \delta I_{ew,u},
\end{aligned} \tag{35}$$

where

$$M^p_{F_{ns},*} \equiv M^p_{F,*} \cot E^p_* \cos A^p_*, \tag{36}$$

$$M^p_{F_{ew},*} \equiv M^p_{F,*} \cot E^p_* \sin A^p_*, \tag{37}$$

and δI_z is the zenith delay, M_F is the mapping function which transforms δI_z into the delay in direction of route. δI_{ns}, δI_{ew} are the north-south and east-west ionosphere gradient vector.

4.3. **Observation equation.** By the linearization of the observation Equations (1)-(4) and revision of ionospheric and tropospheric delays, we can formulate the observation equation as follows:

$$\begin{bmatrix} \tilde{\rho}^{pq}_{CA,uk} \\ \tilde{\rho}^{pq}_{PY,uk} \\ \tilde{\Phi}^{pq}_{L1,uk} \\ \tilde{\Phi}^{pq}_{L2,uk} \end{bmatrix} = \begin{bmatrix} \rho^{pq}_{CA,ku} \\ \rho^{pq}_{PY,ku} \\ \Phi^{pq}_{L1,ku} \\ \Phi^{pq}_{L2,ku} \end{bmatrix} - \left[r^{pq}_{\hat{u}^{(j)}k} + g^{pq}_{\hat{u}^{(j)}k}(-\hat{u}^{(j)}) \right] - [(M^{pq}_{h,k}\delta T_{zh,k} - M^{pq}_{h,u}\delta T_{zh,u}) - (M^{pq}_{w,k}\delta T_{zh,k} - M^{pq}_{w,u}\delta T_{zh,u})]. \tag{38}$$

Applying Equations (29), (35) and (38), we can formulate the observation equation as follows:

$$y_t = H_t \theta_t + v_t, \tag{39}$$

where

$$y \equiv \left[\tilde{\rho}^{\mathrm{T}}_{CA},\ \tilde{\rho}^{\mathrm{T}}_{PY},\ \tilde{\Phi}^{\mathrm{T}}_{L1},\ \tilde{\Phi}^{\mathrm{T}}_{L2}\right]^{\mathrm{T}}, \tag{40}$$

$$H \equiv \left[A,\ B,\ C,\ D\right]^{\mathrm{T}}, \tag{41}$$

$$\theta \equiv [\ u^{\mathrm{T}}, \delta I^{\mathrm{T}}, \delta T^{\mathrm{T}}, \lambda_1 N^{\mathrm{T}}_{L1}, \lambda_2 N^{\mathrm{T}}_{L2}]^{\mathrm{T}}, \tag{42}$$

$$v \equiv [\ e^{\mathrm{T}}_{CA},\ e^{\mathrm{T}}_{PY},\ \lambda_1 \varepsilon^{\mathrm{T}}_{L1}\ \lambda_2 \varepsilon^{\mathrm{T}}_{L2}\ ]^{\mathrm{T}}, \tag{43}$$

$$u \equiv \left[x_u,\ y_u,\ z_u\right]^{\mathrm{T}}, \tag{44}$$

$$A \equiv \left[\ G^{\mathrm{T}}\ G^{\mathrm{T}}\ G^{\mathrm{T}}\ G^{\mathrm{T}}\ \right]^{\mathrm{T}}, \tag{45}$$

$$B \equiv \begin{bmatrix} M_{I,k} & M_{F_{ns},k} & M_{F_{ew},k} & -M_{F_{ns},u} & -M_{F_{ew},u} \\ \frac{{f_1}^2}{{f_2}^2} M_{I,k} & \frac{{f_1}^2}{{f_2}^2} M_{F_{ns},k} & \frac{{f_1}^2}{{f_2}^2} M_{F_{ew},k} & -\frac{{f_1}^2}{{f_2}^2} M_{F_{ns},u} & -\frac{{f_1}^2}{{f_2}^2} M_{F_{ew},u} \\ -M_{I,k} & -M_{F_{ns},k} & -M_{F_{ew},k} & M_{F_{ns},u} & M_{F_{ew},u} \\ -\frac{{f_1}^2}{{f_2}^2} M_{I,k} & -\frac{{f_1}^2}{{f_2}^2} M_{F_{ns},k} & -\frac{{f_1}^2}{{f_2}^2} M_{F_{ew},k} & \frac{{f_1}^2}{{f_2}^2} M_{F_{ew},u} & \frac{{f_1}^2}{{f_2}^2} M_{F_{ew},u} \end{bmatrix}, \tag{46}$$

$$C \equiv \begin{bmatrix} M_{w,k} & -M_{w,u} & M_{T_{ns},k} & M_{T_{ew},k} & -M_{T_{ns},u} & -M_{T_{ew},u} \\ M_{w,k} & -M_{w,u} & M_{T_{ns},k} & M_{T_{ew},k} & -M_{T_{ns},u} & -M_{T_{ew},u} \\ M_{w,k} & -M_{w,u} & M_{T_{ns},k} & M_{T_{ew},k} & -M_{T_{ns},u} & -M_{T_{ew},u} \\ M_{w,k} & -M_{w,u} & M_{T_{ns},k} & M_{T_{ew},k} & -M_{T_{ns},u} & -M_{T_{ew},u} \end{bmatrix}, \tag{47}$$

$$D \equiv \begin{bmatrix} O & O \\ O & O \\ I & O \\ O & I \end{bmatrix}, \quad \delta I \equiv \begin{bmatrix} \delta I^1_{z,ku} \\ \vdots \\ \delta I^{n_s}_{z,ku} \\ \delta I_{ns,k} \\ \delta I_{ew,k} \\ \delta I_{ns,u} \\ \delta I_{ew,u} \end{bmatrix}, \quad \delta T \equiv \begin{bmatrix} \delta T_{z,k} \\ \delta T_{z,u} \\ \delta T_{ns,k} \\ \delta T_{ew,k} \\ \delta T_{ns,u} \\ \delta T_{ew,u} \end{bmatrix}, \tag{48}$$

$$M_{I,k} = \begin{bmatrix} -M^1_{I,k} & M^2_{I,k} & & \\ -M^1_{I,k} & & M^3_{I,k} & \\ \vdots & & & \ddots \\ -M^1_{I,k} & & & M^{n_s}_{I,k} \end{bmatrix}, \tag{49}$$

with definitions of the following vectors:

$$\tilde{\rho}_{CA} \equiv \begin{bmatrix} \tilde{\rho}^{12}_{CA,ku} \\ \vdots \\ \tilde{\rho}^{1n_s}_{CA,ku} \end{bmatrix}, \quad \tilde{\rho}_{PY} \equiv \begin{bmatrix} \tilde{\rho}^{12}_{PY,ku} \\ \vdots \\ \tilde{\rho}^{1n_s}_{PY,ku} \end{bmatrix}, \quad \tilde{\Phi}_{L1} \equiv \begin{bmatrix} \tilde{\Phi}^{12}_{L1,ku} \\ \vdots \\ \tilde{\Phi}^{1n_s}_{L1,ku} \end{bmatrix},$$

$$\tilde{\Phi}_{L2} \equiv \begin{bmatrix} \tilde{\Phi}^{12}_{L2,ku} \\ \vdots \\ \tilde{\Phi}^{1n_s}_{L2,ku} \end{bmatrix}, \quad M_{F_{ns},*} \equiv \begin{bmatrix} M^{12}_{F_{ns},*} \\ \vdots \\ M^{1n_s}_{F_{ns},*} \end{bmatrix}, \quad M_{F_{ew},*} \equiv \begin{bmatrix} M^{12}_{F_{ew},*} \\ \vdots \\ M^{1n_s}_{F_{ew},*} \end{bmatrix},$$

$$M_{T_{ns},*} \equiv \begin{bmatrix} M^{12}_{T_{ns},*} \\ \vdots \\ M^{1n_s}_{T_{ns},*} \end{bmatrix}, \quad M_{T_{ew},*} \equiv \begin{bmatrix} M^{12}_{T_{ew},*} \\ \vdots \\ M^{1n_s}_{T_{ew},*} \end{bmatrix}, \quad M_{w,*} \equiv \begin{bmatrix} M^{12}_{w,*} \\ \vdots \\ M^{1n_s}_{w,*} \end{bmatrix},$$

$$N_{L1} \equiv \begin{bmatrix} N^{12}_{L1,ku} \\ \vdots \\ N^{1n_s}_{L1,ku} \end{bmatrix}, \quad N_{L2} \equiv \begin{bmatrix} N^{12}_{L2,ku} \\ \vdots \\ N^{1n_s}_{L2,ku} \end{bmatrix}, \quad e_{CA} \equiv \begin{bmatrix} e^{12}_{CA,ku} \\ \vdots \\ e^{1n_s}_{CA,ku} \end{bmatrix},$$

$$e_{PY} \equiv \begin{bmatrix} e^{12}_{PY,ku} \\ \vdots \\ e^{1n_s}_{PY,ku} \end{bmatrix}, \quad \varepsilon_{L1} \equiv \begin{bmatrix} \varepsilon^{12}_{L1,ku} \\ \vdots \\ \varepsilon^{1n_s}_{L1,ku} \end{bmatrix}, \quad \varepsilon_{L2} \equiv \begin{bmatrix} \varepsilon^{12}_{L2,ku} \\ \vdots \\ \varepsilon^{1n_s}_{L2,ku} \end{bmatrix},$$

where "$*$" is "k" or "u". G is a partial differentiation coefficient procession

$$G \equiv \left[\; g^{12}_{\hat{u}(j)}, g^{13}_{\hat{u}(j)}, \ldots, g^{1n_s}_{\hat{u}(j)} \; \right]^{\mathrm{T}}, \tag{50}$$

that is

$$G = \begin{bmatrix} \dfrac{\partial r^{12}_{\hat{u}(j)k}}{\partial \hat{x}_{u(j)k}} & \dfrac{\partial r^{12}_{\hat{u}(j)k}}{\partial \hat{y}_{u(j)k}} & \dfrac{\partial r^{12}_{\hat{u}(j)k}}{\partial \hat{z}_{u(j)k}} \\ \dfrac{\partial r^{13}_{\hat{u}(j)k}}{\partial \hat{x}_{u(j)k}} & \dfrac{\partial r^{13}_{\hat{u}(j)k}}{\partial \hat{y}_{u(j)k}} & \dfrac{\partial r^{13}_{\hat{u}(j)k}}{\partial \hat{z}_{u(j)k}} \\ \vdots & \vdots & \vdots \\ \dfrac{\partial r^{1n_s}_{\hat{u}(j)k}}{\partial \hat{x}_{u(j)k}} & \dfrac{\partial r^{1n_s}_{\hat{u}(j)k}}{\partial \hat{y}_{u(j)k}} & \dfrac{\partial r^{1n_s}_{\hat{u}(j)k}}{\partial \hat{z}_{u(j)k}} \end{bmatrix}$$

$$= \begin{bmatrix} \dfrac{\hat{x}_u - x^1}{\hat{r}^1_u} - \dfrac{\hat{x}_u - x^2}{\hat{r}^2_u} & \dfrac{\hat{y}_u - y^1}{\hat{r}^1_u} - \dfrac{\hat{y}_u - y^2}{\hat{r}^2_u} & \dfrac{\hat{z}_u - z^1}{\hat{r}^1_u} - \dfrac{\hat{z}_u - z^2}{\hat{r}^2_u} \\ \vdots & \vdots & \vdots \\ \dfrac{\hat{x}_u - x^1}{\hat{r}^1_u} - \dfrac{\hat{x}_u - x^{n_s}}{\hat{r}^{n_s}_u} & \dfrac{\hat{y}_u - y^1}{\hat{r}^1_u} - \dfrac{\hat{y}_u - y^{n_s}}{\hat{r}^{n_s}_u} & \dfrac{\hat{z}_u - z^1}{\hat{r}^1_u} - \dfrac{\hat{z}_u - z^{n_s}}{\hat{r}^{n_s}_u} \end{bmatrix}. \tag{51}$$

5. **Kalman Filter.** The Kalman filter [15, 16] is applied to estimate the unknown vecter $\boldsymbol{\theta}$. The measurement equation is shown in Equation (39), and the state equation can be generally expressed as follows.

$$\theta_{t+1} = F\theta_t + w_t, \qquad t = 0, 1, 2, \cdots, \tag{52}$$

where F is a known matrix with appropriate dimensions. And w_t and v_t are assumed to be white Gaussian processes, such that

$$\mathrm{E}\{w_t\} = 0, \qquad \mathrm{E}\{v_t\} = 0 \tag{53}$$

$$\mathrm{E}\left\{ \begin{pmatrix} w_t \\ v_t \end{pmatrix} \begin{pmatrix} w_s^{\mathrm{T}} & v_s^{\mathrm{T}} \end{pmatrix} \right\} = \begin{pmatrix} Q & 0 \\ 0 & R \end{pmatrix} \delta_{ts} \tag{54}$$

$$\mathrm{E}\{w_t\,\theta_s^{\mathrm{T}}\} = 0, \qquad \mathrm{E}\{v_t\,\theta_s^{\mathrm{T}}\} = 0, \quad s \le t \tag{55}$$

$$\theta_0 \sim N(\bar{x}_0, \Sigma_0) \tag{56}$$

Then the Kalman filter algorithm can be shown as follows:

1) Predicted and Filtered Estimates

$$\hat{\theta}_{t+1|t} = F\hat{\theta}_{t|t}, \tag{57}$$

$$\hat{\theta}_{t|t} = \hat{\theta}_{t|t-1} + K_t \left[y_t - H\hat{\theta}_{t|t-1} \right]. \tag{58}$$

2) Filter Gain (Kalman Gain)

$$K_t = P_{t|t-1} H^{\mathrm{T}} \left[H P_{t|t-1} H^{\mathrm{T}} + R \right]^{-1}. \tag{59}$$

3) Predicted and Filtered Error Covariance Matrices

$$P_{t+1|t} = F P_{t|t} F^{\mathrm{T}} + Q, \tag{60}$$

$$P_{t|t} = P_{t|t-1} - K_t H P_{t|t-1}. \tag{61}$$

4) Initial Conditions

$$\hat{\theta}_{0|-1} = \bar{\theta}_0, \qquad P_{0|-1} = \Sigma_0. \tag{62}$$

6. **Experiments.** The experiment of the proposed positioning algorithms was carried out by using real receiver data. The observation data were obtained from four GEONET reference stations (OTSU1 in Shiga, Japan, YASU in Shiga, Japan, HIMEZI in Hyogo, Japan and FUJI in Shizuoka, Japan.). The coordinates of these stations are shown in Table 1. Figure 3 shows the locations of the used stations. In the experiments, results of two methods were compared. Method 1 estimated only the zenith total delays of the ionospheric and tropospheric delays (our previous results [6]). Method 2 estimated the both of zenith total delays and their gradients (results by the algorithm proposed in this paper). Table 2 summarizes the estimation methods. The results of method 1 were plotted by red points and the method 2 were plotted by blue points throughout the following section.

TABLE 1. Receiver positions

Station	Lat. [deg.]	Lon. [deg.]	Ell. Height [m]
OTSU1	35.13703982	135.87080794	220.3448
YASU	35.08572344	136.04119882	134.9507
HIMEZI	34.86412096	134.65966396	68.5357
FUJI	35.17358988	138.72154156	133.9394

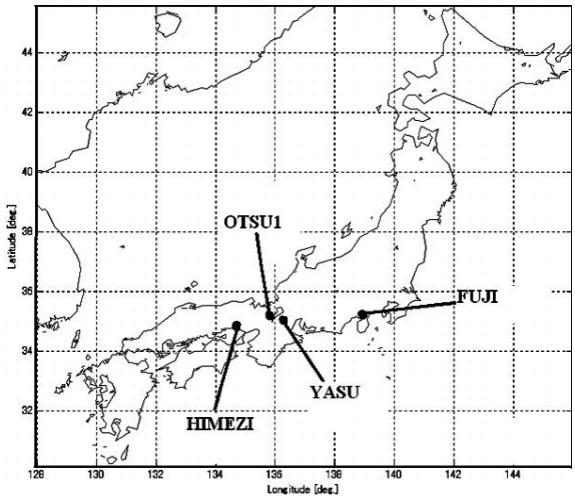

FIGURE 3. Locations

TABLE 2. Estimation methods

method 1	Ionospheric and Tropospheric delays	Zenith total delays
method 2	Ionospheric and Tropospheric delays	Zenith + Gradients

TABLE 3. Datasets for static tests

Dataset	Station		Time (UTC)
A	Rov.	OTSU1	2008.Aug.1 (00:00 ∼ 23:59'30) Interval: 30 [sec]
	Ref.	YASU	
	Baseline	16.545 [km]	
B	Rov.	OTSU1	
	Ref.	HIMEZI	
	Baseline	114.633 [km]	
C	Rov.	OTSU1	
	Ref.	FUJI	
	Baseline	259.758 [km]	

6.1. **Results.** In the experiments, three datasets and two methods were used as shown in Table 3. An elevation cut-off angle of 15 degrees was applied to these data. At every station, the Trimble 5700 receiver with the TRM29659.00 antenna observed L1 and L2 carrier phases and C/A and P(Y) code pseudoranges at every 30 seconds. For implementing the Kalman filter, the dynamical models for state variables and initial conditions are shown in the following Table 4. The initial values of the unknown position u was obtained by the standard point positioning method [4, 5], the ionospheric delay δI by Klobuchar model, the tropospheric delay δT by Saastamoinen model of Equation (24) and the ambiguity N_{L1}, N_{L2} by subtracting the measurement of Equation (1) from Equation (3).

6.1.1. *Results for dataset A (16.545 [km] baseline).* Figure 4 shows the results for the dataset A, short baseline (16.545 [km]). The blue and red lines show the positioning errors along with the local level axes (East, North and Up), where the errors were computed

TABLE 4. State model and initial condition

State variable	Dynamical model	Initial Condition	
		Initial value	Std. Dev.
Position (u)	Constant	Point Pos.	10
Ionosphere (δI)	Brownian	Klobuchar	1.0
Troposphere δT	Brownian	2.4	0.03
Ambiguity ($\lambda_1 N_{L1}, \lambda_2 N_{L2}$)	Constant	$\Phi_{dd} - \rho_{dd}$	10

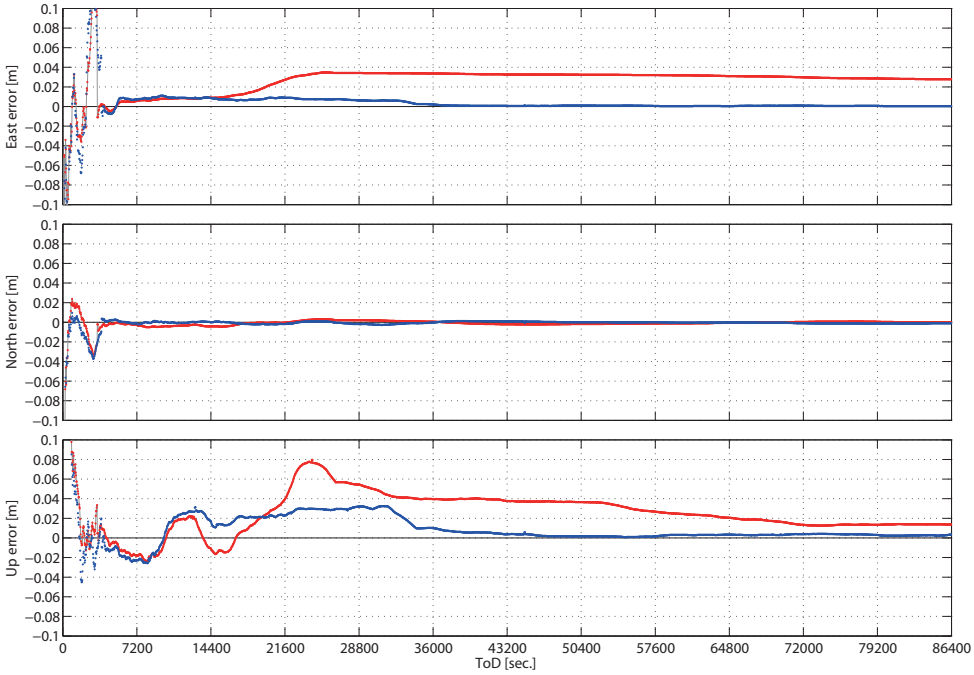

FIGURE 4. ENU errors (Aug.1, baseline length: 16.545 [km])

TABLE 5. Summary statistics (baseline length: 16.545 [km])

Method	Dir.	Bias [m]	STD [m]	RMS [m]
method 1	East	0.0300	0.0056	0.0306
	North	−0.0004	0.0015	0.0015
	Up	0.0299	0.0178	0.0348
method 2	East	0.0025	0.0029	0.0039
	North	−0.0005	0.0010	0.0011
	Up	0.0096	0.0103	0.0140

by differencing the estimated positions from the positions in Table 1. The statistics of positioning results are summarized in Table 5. The results were calculated time from 7200 to 86400 [sec].

6.1.2. *Results for dataset B (114.633 [km] baseline).* Figure 5 shows the results for the dataset B, medium baseline (114.633 [km]). The blue and red lines show the positioning errors along with the local level axes (East, North and Up), where the errors were computed by differencing the estimated positions from the positions in Table 1. The statistics

of positioning results are summarized in Table 6. The results were calculated time from 7200 to 86400 [sec].

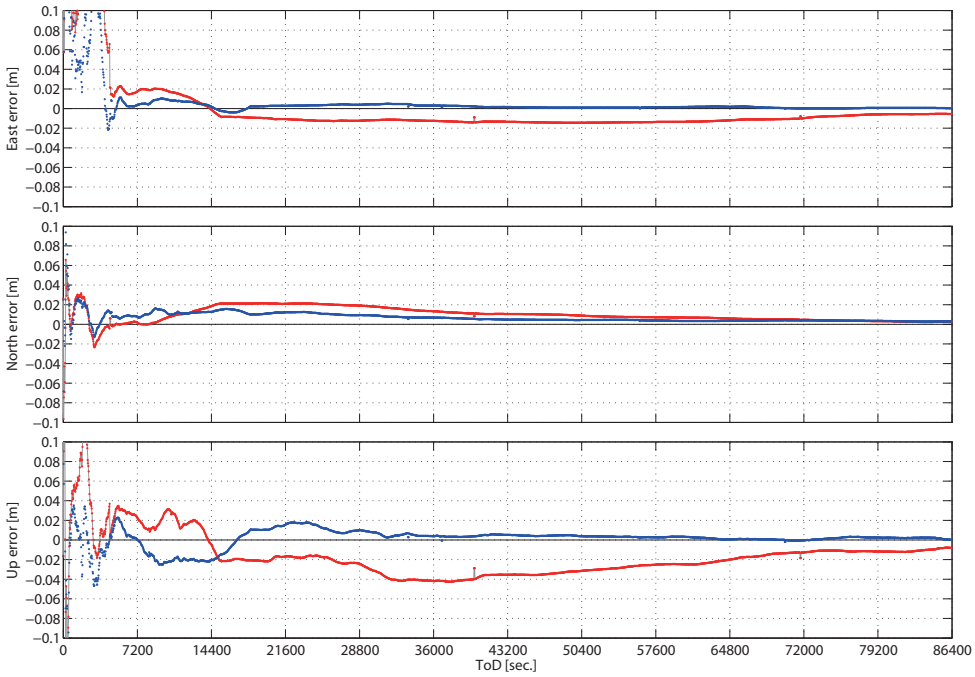

FIGURE 5. ENU errors (Aug.1, baseline length: 114.633 [km])

TABLE 6. Summary statistics (baseline length: 114.633 [km])

Method	Dir.	Bias [m]	STD [m]	RMS [m]
method 1	East	−0.0113	0.0027	0.0116
	North	0.0108	0.0063	0.0125
	Up	−0.0244	0.0100	0.0264
method 2	East	0.0016	0.0016	0.0023
	North	0.0061	0.0033	0.0070
	Up	0.0040	0.0053	0.0066

6.1.3. *Results for dataset C (259.758 [km] baseline).* Figure 6 shows the results for the dataset C, long baseline (259.758 [km]). The blue and red lines show the positioning errors along with the local level axes (East, North and Up), where the errors were computed by differencing the estimated positions from the positions in Table 1. The statistics of positioning results are summarized in Table 7. The results were calculated time from 14400 to 86400 [sec].

In this experiments, it was quite effective to estimate ionospheric and tropospheric gradients when we focus on estimating their delays in various baselines. Especially ionosphere can be active, therefore the estimating so effective.

7. **Conclusions.** In this paper, the relative positioning algorithms with estimating ionospheric and tropospheric delays and their gradients have been proposed. The algorithms are applied by the Kalman filter. Examinations of the algorithms were done by using real receiver data of GEONET. Our experimental results show that, in the static situation, the

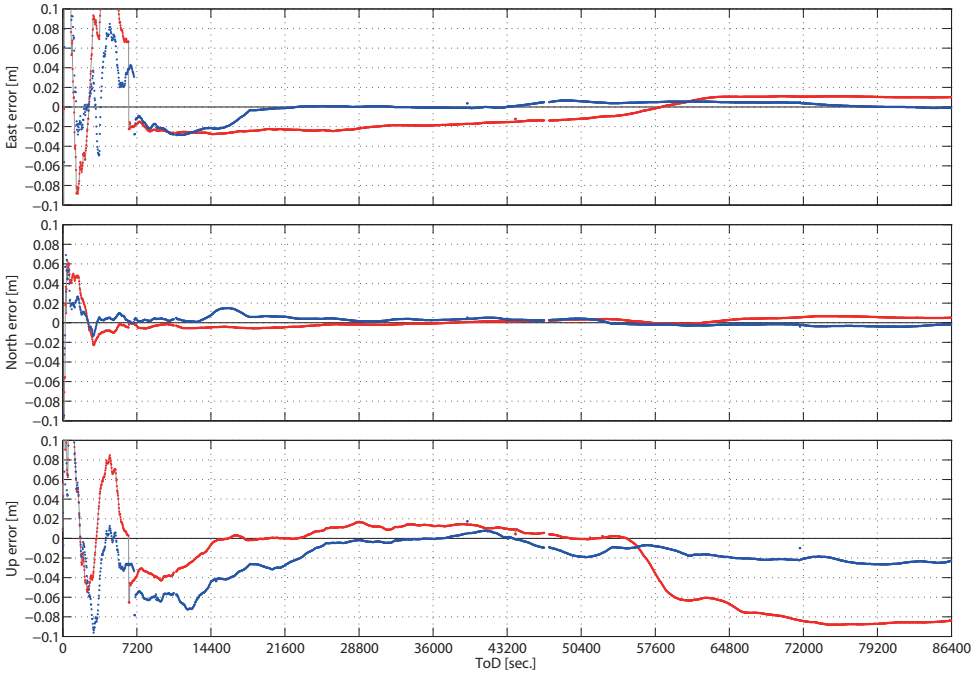

FIGURE 6. ENU errors (Aug.1, baseline length: 259.758 [km])

TABLE 7. Summary statistics (baseline length: 259.758 [km])

Method	Dir.	Bias [m]	STD [m]	RMS [m]
method 1	East	−0.0075	0.0140	0.0159
	North	0.0011	0.0035	0.0037
	Up	−0.0260	0.0409	0.0485
method 2	East	0.0010	0.0050	0.0052
	North	0.0013	0.0041	0.0044
	Up	−0.0143	0.0115	0.0183

proposed algorithm with estimating ionospheric and tropospheric gradients can achieve more accurate positioning than without gradients estimation.

REFERENCES

[1] C. Uratani, K. Sone, Y. Muto, S. Maruo and S. Sugimoto, Dynamical models for carrier-phase kinematic GPS positioning, *Proc. of the 16th Int. Tech. Meeting of the Satellite Division of the Institute of Navigation (ION GPS/GNSS)*, Portland, OR, pp.809-818, 2003.

[2] Y. Muto, Y. Kubo, C. Uratani and S. Sugimoto, New dynamical models for kinematic GPS positioning, *Proc. of the 17th Int. Tech. Meeting of the Satellite Division of the Institute of Navigation (ION GNSS)*, Long Beach, CA, pp.2519-2528, 2004.

[3] S. Kitao, Y. Kubo, Y. Muto and S. Sugimoto, Dynamical models with constraint for precise RTK positioning, *Proc. of the 18th Int. Tech. Meeting of the Satellite Division of the Institute of Navigation (ION GNSS)*, Long Beach, CA, pp.1555-1563, 2005.

[4] B. W. Parkinson and J. J. Spilker Jr. (eds.), *Global Positioning System: Theory and Applications*, vol.1-2, AIAA, Washington D.C., 1997.

[5] P. Misra and P. Enge, *Global Positioning System – Signals, Measurements, and Performance*, 2nd Edition, Ganga-Jamuna Press, Massachusetts, 2006.

[6] T. Yanase, S. Fujita, H. Tanaka, Y. Kubo and S. Sugimoto, Long baseline GNSS relative positioning with estimating zenith delays of ionospheric and tropospheric delays, *Proc. of International Symposium on GPS/GNSS*, Jeju, pp.185, 2009.

[7] K. Nishikawa, S. Fujita, Y. Kubo and S. Sugimoto, PPP based on GR models with estimating tropospheric and ionospheric delays, *Proc. of the 22th Int. Tech. Meeting of the Satellite Division of the Institute of Navigation (ION GNSS)*, Savannah, GA, pp.2496-2507, 2009.

[8] E. K. Smith and S. Weintraubz, The constants in the equation for atmospheric refractive index at radio frequencies, *Proc. of IRE*, vol.41, pp.1035-1037, 1953.

[9] J. A. Klobuchar, Ionospheric time-delay algorithm for single-frequency GPS users, *IEEE Trans. on Aerospace and Electronic Systems*, vol.AES-23, no.3, pp.325-331, 1987.

[10] S. Fujita, Y. Kubo and S. Sugimoto, Ionosphere total electron content estimation based on GR models at known positions, *International Journal of Innovative Computing, Information and Control*, vol.5, no.1, pp.139-152, 2009.

[11] S. Sugimoto, Y. Kubo and H. Kumagai, GPS navigation algorithms and estimation – Detection theory, *Systems, Control and Information ISCIE*, vol.46, no.5, pp.276-285, 2002 (in Japanese).

[12] B. Hofmann-Wellenhof, H. Lichtenegger and J. Collins, *Global Positioning System Theory and Practice*, 5th Edition, Springer-Verlag, New York, 2001.

[13] J. Saastamoinen, Contributions to the theory of atmospheric refraction, part 2, *Geodesique*, vol.107, pp.13-34, 1972.

[14] K. Chen and Y. Gao, Ionospheric effect mitigation for real-time single-frequency precise point positioning, *The Institute of Navigation*, vol.55, no.3, pp.205-213, 2008.

[15] A. Gelb (ed.), *Applied Optimal Estimation*, MIT Press, Massachusetts, 1974.

[16] R. G. Brown and P. Y. C. Hwang, *Introduction to Random Signals and Applied Kalman Filtering*, 3rd Edition, John Wiley & Sons, New York, 1997.